Extreme Mechanics Letters 25 (2018) 1–6

Contents lists available at ScienceDirect

Extreme Mechanics Letters

journal homepage: www.elsevier.com/locate/eml

Buckling and post-buckling of an elastic rod embedded in a bilayer matrix

Dong Wang [a], Nan Hu [b], Shicheng Huang [c], Amir Mohammadi Nasab [d], Kevin Yang [c], Matthew C. Abate [c], Xiaojiao Yu [c], Likun Tan [c], Wanliang Shan [d], Zi Chen [c,*]

[a] School of Mechanical Engineering, Shanghai Jiao Tong University, Shanghai 200240, China
[b] Civil, Environmental and Geodetic Engineering, The Ohio State University, 470 Hitchcock Hall, 2070 Neil Ave, Columbus, OH 43210, United States
[c] Thayer School of Engineering, Dartmouth College, Hanover, NH 03755, USA
[d] Department of Mechanical Engineering, University of Nevada, Reno, NV 89557, USA

ARTICLE INFO

Article history:
Received 13 August 2018
Received in revised form 14 October 2018
Accepted 14 October 2018
Available online 19 October 2018

Keywords:
Buckling
Elastic medium
Bilayer

ABSTRACT

Many biological and engineered systems can be modeled as buckled thin rods with constraints. Examples include microtubules in cytoskeleton, plant roots in soil, and oil pipes within a wellbore. However, most previous studies focused on the buckling of a rod in a homogeneous environment, an idealization which is often not realistic. Here, we study the buckling behaviors of an elastic rod embedded in a bilayer elastic matrix using a combined experimental, theoretical, and computational method. Our experiments showed, for the first time, that the buckling amplitude can increase from the end where the compressive load is applied. To interpret this new phenomenon, we built a theoretical model and identified an ansatz for the transverse displacement. Our numerical results showed that material inhomogeneity, geometry, and loading all have significant influences on the post-buckling behaviors of the rod. Moreover, our study indicated that the stiffer layer of the elastic medium can be treated as a clamped boundary. These results could find applications ranging from the penetration of needles through biological tissues to the development of underground structures.

1. Introduction

Many deformed structures in nature and engineering are analogous to an elastic rod embedded in an elastic medium, e.g., microtubules supported by cytoplasm in living cells [1–5], plant roots grown in soil [6], electrodes embedded in brain tissues for deep brain stimulation [7], and pipelines on the seabed [8,9]. The buckling behaviors of these structures have drawn considerable attention in recent years to identify the effects of the medium on the deformation of the rod. It was shown that a rod embedded in an elastic matrix buckles into a pattern with a large wave number, and hence sustains significantly higher compressive loads than otherwise [10,11]. In fact, it was found that a cytoskeleton matrix allows the microtubules of whole cells to withstand as much as one hundred times more compressive force than they could in the absence of an elastic network [2].

A number of models have been developed to investigate the buckling of rods in an homogeneous isotropic elastic medium. For example, the buckling of microtubules was studied within a network of intermediate filaments [12], and three different lateral support conditions were considered: unsupported, continuous elastic support, and rigid support at irregular intervals. Later, the microtubules in cell cytoskeleton were shown to be able to withstand significantly higher compressive forces, and the results were confirmed experimentally and theoretically [2]. A following work examined the force propagation along an elastic rod embedded in a non-linear elastic matrix by taking into account both linear and nonlinear effects [13]. However, in these previous studies, researchers neither considered nor showed any variation in buckling amplitudes. The buckling amplitude was revealed to decay exponentially away from the end through both experiments and theory, where the compressive load is applied by considering not only the transverse coupling but also the longitudinal coupling between the rod and its surrounding medium [14]. More recent studies include buckling of rods due to growth [15] and buckling of beam under two lateral constraints [16].

While the surrounding medium was assumed to be homogeneous in most studies [2,12–14], this assumption is typically an oversimplification. For example, the cytoskeleton that supports microtubules is not homogeneous [17]; the terrestrial environment in which plant roots grow is heterogeneous [18]; the tissues that surround blood vessels are heterogeneous in nature [19]; and the composition of the seabed that pipelines rest on varies [20].

* Corresponding author.
E-mail addresses: wang_dong@sjtu.edu.cn (D. Wang), Hu.1773@osu.edu (N. Hu), zi.chen@dartmouth.edu (Z. Chen).

https://doi.org/10.1016/j.eml.2018.10.004
2352-4316/

The effects of heterogeneous surrounding media remain poorly understood, as only a few studies touched on this type of problem, e.g., plant root buckling in a bilayer hydrogel medium [6] and buckling of elastic beams in granular media [21].

In this paper, we first showed through experiments that the buckling amplitude can increase from the end where the longitudinal force is applied, in sharp contrast to previous findings [2,13,14]. To interpret this counter-intuitive phenomenon, we built a theoretical model for an elastic rod embedded in a bilayer elastic matrix under compressive loading and obtained analytical solutions within the framework of a variational theory. This work focuses on the buckling shape and critical buckling load at the onset of buckling. For simplicity, here we consider the buckling of a thin elastic in a bilayer elastic medium. Nevertheless, this approach can be generalized to study the buckling of a rod in a multilayer medium.

2. Experiments and model

We started by experimentally investigating the buckling behavior of a rod embedded in bilayered elastic medium as shown in Fig. 1(a), (c) and movie S1. 40 g/L and 60 g/L gelatins were used to build the bilayer elastic medium. Superelastic nitinol wires (55% nickel, 45% titanium) with diameter 457.2 μm obtained from Small Parts, Inc were used. The Young's modulus of the rod was found to be $E = 60.8 \pm 1.0$ GPa in a previous study [14]. The experiments used porcine gelation (Sigma Aldrich) at a concentration of 40 g/L for the top layer and 60 g/L for the bottom layer. The gelatin in the study was made by dissolving gelatin powder into filtered water. The samples were cooled to and held at 5 °C for 12–24 h to allow for gelling. The length and diameter of the test tube is 220 mm and 30 mm respectively. For comparison, the buckling behaviors of the rods embedded in 40 g/L or 60 g/L single layer gelatins were shown in Fig. 1(e) and (f), respectively.

It was found that the buckling amplitude of the rod could increase away from the loading point when the rod is embedded in bilayered medium as shown in Fig. 1(c) , in contrast with the decreasing behavior in previous studies [13,14] as exemplified in Fig. 1(e) and (f). In order to understand this phenomenon, we consider the buckling behavior of an elastic, isotropic, long rod embedded in a bilayer elastic matrix. The schematic illustration of a rod embedded in bilayered matrix is shown in Fig. 1(g). Both layers of the elastic media are isotropic, homogeneous and elastic with different stiffness α_1 and α_2. The length of the elastic media in x-direction is l_1 and l_2, respectively. A compressive force p is applied at the top end of the rod. The deformation in the longitudinal direction is assumed to be small. The displacement of the rod and the angle between the rod's tangential direction and longitudinal direction are continuous through the interface of the two layer matrix. The governing equations of the rod in each layer are derived using the variational method.

The total potential energy of the system U_T can be described as

$$U_T = -p\int_0^{l_1+l_2}\frac{1}{2}(u')^2dx + \int_0^{l_1+l_2}\frac{\kappa}{2}(u'')^2dx + \frac{\alpha_1}{2}\int_0^{l_1}(u)^2dx + \frac{\alpha_2}{2}\int_{l_1}^{l_2}(u)^2dx, \quad (1)$$

where $u(x)$ is the transverse displacement of the rod as a function of the axial coordinate x; α_1 and α_2 represent the stiffness of the first- and second-layer of the elastic media. $\kappa = EI$ is the bending modulus of the rod, where E is the Young's modulus and I is the area moment of inertia. The first term represents the axial compression energy released by the buckling, the second term represents the bending energy of the rod, and the last two terms are the elastic strain energy associated with lateral deformation into the surrounding medium. Here the rod is still assumed to be long enough, but longitudinal coupling is not considered, unlike in previous studies [13,14]. In what follows, we will show that this inhomogeneity in matrix will also lead to wave amplitude changes.

Table 1
Parameters used in Fig. 1(a/b) and (c/d).

	Fig. 1(a/b)	Fig. 1(c/d)
κ	1.304×10^{-4}	1.304×10^{-4}
Layer 1 concentration	Gelatin 40 g/L	Gelatin 60 g/L
Layer 2 concentration	Gelatin 60 g/L	Gelatin 40 g/L
l_1	125 mm	130 mm
l_2	95 mm	90 mm
α_1	73 Pa	313 Pa
α_2	350 Pa	104 Pa
δL	0.9 mm	1.0 mm

Using the variational method,

$$\delta U_T = 0, \quad (2)$$

the following governing equations for the two layers can be obtained as:

$$p\frac{d^2u_i}{dx^2} + \alpha_i u_i + \kappa\frac{d^4u_i}{dx^4} = 0 \quad (i = 1, 2), \quad (3)$$

where p is the applied compressive force.

The above governing equations can be non-dimensionalized as:

$$P\frac{d^2U_i}{dX^2} + A_i U_i + \frac{d^4U_i}{dX^4} = 0 \quad (i = 1, 2), \quad (4)$$

using

$$U_i = u_i/l_r;\ X = x/l_r;\ P = l_r^2 p/\kappa;$$
$$A_1 = \alpha_1 l_r^4/\kappa;\ A_2 = \alpha_2 l_r^4/\kappa. \quad (5)$$

Here, l_r is chosen as half of the length of the rod, i.e., $l_r = (l_1+l_2)/2$. The length of the first layer and second layer elastic medium is normalized as: $L_1 = l_1/l_r$ and $L_2 = l_2/l_r$. The normalized total length of the rod is then $L_1 + L_2 = 2$.

Solving the governing equation for each layer, the general solution of the above fourth-order ODE is obtained as:

$$U_i = C_{i1}cos(\sqrt{m_i}x) + C_{i2}cos(\sqrt{n_i}x) + C_{i3}sin(\sqrt{m_i}x) + C_{i4}sin(\sqrt{n_i}x) \quad (i = 1, 2) \quad (6)$$

with

$$m_i = \frac{P - \sqrt{P^2 - 4A_i}}{2},\ n_i = \frac{P + \sqrt{P^2 - 4A_i}}{2}. \quad (7)$$

There are eight unknown constants C_{i1}, C_{i2}, C_{i3}, C_{i4}, $i = 1,2$, which are solved using pinned–pinned boundary conditions as indicated in the Supplementary Material.

The critical buckling load is obtained in the Supplementary Material as:

$$P_{cr} = min\{\sqrt{4A_1}, \sqrt{4A_2}\}. \quad (8)$$

In the case of rod buckling in homogeneous elastic media, i.e., $A_1 = A_2 = A$, the critical buckling load is $P_{cr} = \sqrt{4A}$. Transforming the above results back to dimensional parameters, $p_{cr} = \sqrt{4\kappa\alpha}$, where $\alpha_1 = \alpha_2 = \alpha$. The above result is consistent with the prior works [2,13,14]. The results show that the part of the rod embedded in the softer elastic medium will buckle first when the compressive force reaches its critical buckling load $min\{\sqrt{4\alpha_1\kappa}, \sqrt{4\alpha_2\kappa}\}$. It will then cause the part of the rod embedded in stiffer elastic matrix to buckle, which would otherwise be straight if the rod is embedded in the homogeneous stiffer elastic medium.

Next, we compare the experimental, theoretical, and numerical shapes of the rods embedded in 40 g/L (top)–60 g/L (bottom) gelatin bilayer (Fig. 1(b)) and 60 g/L–40 g/L gelatin bilayer

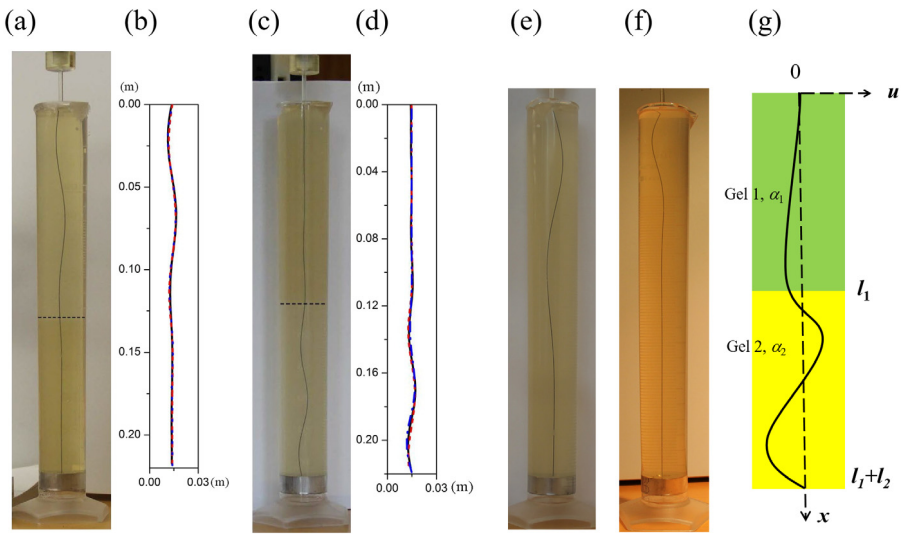

Fig. 1. Image of the experimental setup showing a compressed wire embedded in (a) 40 g/L (top)–60 g/L (bottom) bilayer, (c) 60 g/L (top)–40 g/L (bottom) bilayer, (e) 40 g/L single layer and (f) 60 g/L single layer . (b)/(d) The theoretical results (red), finite element simulation (blue) and experimental profile (black) of the wire in (a)/(c). (g) Schematic illustration of an elastic rod embedded within a bilayer elastic medium.

(Fig. 1(d)), respectively. The black solid curve represents the experimental shape, the red dotted curve is the predicted shape using the theoretical model, and the blue curve represents Abaqus simulation results. The parameters used in the model can be found in Table 1. The stiffness α of the 40 g/L gelatin is estimated to be between 73 and 104 Pa, while that of the 60 g/L gelatin is between 313 and 350 Pa. By using the estimated stiffness of the gelatin, the wavelength of the same rod embedded in the single layer gelatin is calculated as 88 mm for 40 g/L gelatin and 63 mm for 60 g/L gelatin according to the method in [22], which agree reasonably with experiments (not shown here). As can be seen from Fig. 1, predicted shapes are in excellent agreement with experiments. There is some discrepancy between the shapes, notably at the interface between the two gelatin layers. The slight discrepancy can be attributed to (a) the lateral displacement at the loading point in experiments; (b) the longitude displacement at the loading point, which is not accounted for in the model; (c) the decay of the longitude force, not taken into account into the model; (4) the transition at the interface, which is assumed to be continuous in the model. A transition zone may exist in experiments due to the inhomogeneity at the interface. It is also worth mentioning that the total longitude displacement is 0.9 and 1.0 mm for Fig. 1(a) and (c) respectively, which is small compared to the length of the rod $\sim$ 220 mm.

3. Numerical results

To determine the quantitative relation between a rod's buckled profile and its geometric and mechanical properties, a series of tests were performed following the theoretical framework proposed. Specifically, this section investigates the dependences of the buckled shape on the elastic stiffness of the bilayer medium, interface position and applied force. The parameters used in this section are all normalized.

3.1. Effect of the stiffness ratio of the bilayer elastic media

First, we studied how the stiffness ratio of the bilayer influences the bilayer shape. Fig. 2(a) plots the deformation of the rod for different stiffness ratios $A_2/A_1 = 1, 1.1, 2, 10, 50$. Here A_1 is fixed as 1000 and A_2 is changing for different curves. $L_1 = L_2 = 1$. The total longitudinal displacement $\int_0^{L_1+L_2} \frac{1}{2}(U')^2 dX$ is fixed as 0.005. The normalized compressive force P is chosen as the critical buckling load $2\sqrt{1000} \approx 64$. The shape of the rod is symmetric at the interface ($A_2/A_1 = 1$), when embedded in a homogeneous elastic matrix. However, this symmetry is broken even for small heterogeneity of the elastic matrix ($A_2/A_1 = 1.1$), and the amplitude in layer 1 increases and in layer 2 decreases. As the stiffness ratio increases, the amplitude of U in layer 2 decreases and the length of the wave in layer 1 decreases as new waves are generated at the end of the rod. When the stiffness ratio is very large, ($A_2/A_1 = 50$), the displacement in layer 2 is very small and can be neglected. Thus layer 2 can be regarded as an additional boundary condition, and therefore the original pinned boundary condition at $X = 2$ becomes equivalent to a clamped boundary condition. It should be mentioned that as the ratio increases from 1.1 to 50, the maximum amplitude of U in layer 1 undergoes almost no change.

Both experimental and theoretical results suggest that the stiffer layer can be regarded as an additional clamped boundary condition. Fig. 2(b) plots the position of 95% of longitudinal displacement $L_{0.95}$ against A_2/A_1 with $A_1 = 10$, 100, 1000 and 10 000. The other parameters used in this figure are the same as those in Fig. 2(a). The $L_{0.95}$ is defined as the point that makes $\int_0^{L_{0.95}} (U')^2 dX / \int_0^{L_t} (U')^2 dX = 95\%$, which means that 95% of the longitudinal displacement exists from 0 to $L_{0.95}$. Thus, the part of elastic medium from $L_{0.95}$ to 2 can be considered as an additional clamped boundary condition. It can be seen that $L_{0.95}$ generally decreases monotonically with A_2/A_1, which means that a stiffer second layer works better as an additional clamped boundary condition. $L_{0.95}$ depends not only on the ratio of A_2/A_1, but also on the value of stiffness A_1 or A_2. For the same A_2/A_1 ratio, a larger A_1 will lead to a smaller $L_{0.95}$. When A_1 is large ($A_1 = 1000$ or 10 000), $L_{0.95}$ drops rapidly at the beginning. Taking the curve with $A_1 = 10\,000$ as example, $L_{0.95} = 1.913$ at $A_2/A_1 = 1$ and it drops to 1.208 at $A_2/A_1 = 1.6$. Thus the stiffer layer can be regarded as an additional clamped boundary condition, even for relatively small stiffness ratios A_2/A_1 with large A_1.

3.2. Effect of the stiffness ratio of the elastic media to rod

To illustrate the dependence of the rod shape on the elastic matrix stiffness, U is plotted versus X for different elastic media stiffness $A_2 = 10$, 100, 1000, 10 000, 100 000 with $A_1/A_2 = 2$

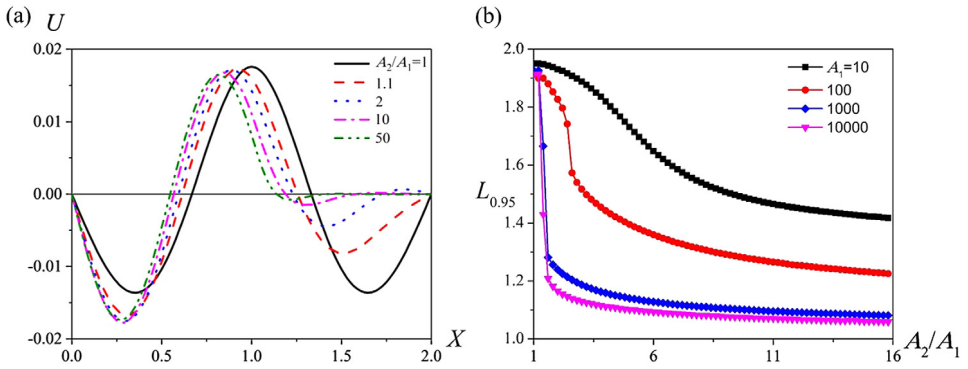

Fig. 2. (a) The deformation of the rod for different layer stiffness ratios $A_2/A_1 = 1, 1.1, 2, 10, 50$ with $A_1 = 1000$. (b) The dependence of the percentage of the second layer displacement in the total displacement $\int_{L_1}^{L_t}(U')^2dX/\int_0^{L_t}(U')^2dX$ on A_2/A_1 at the onset of buckling.

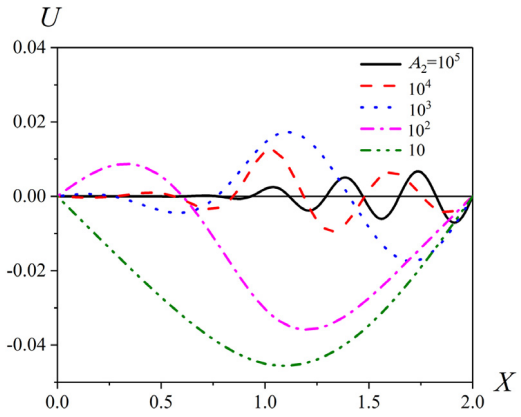

Fig. 3. The shape of a rod embedded in an elastic matrix with different stiffness A_2 with $A_1/A_2 = 2$. The interface is at X = 1.

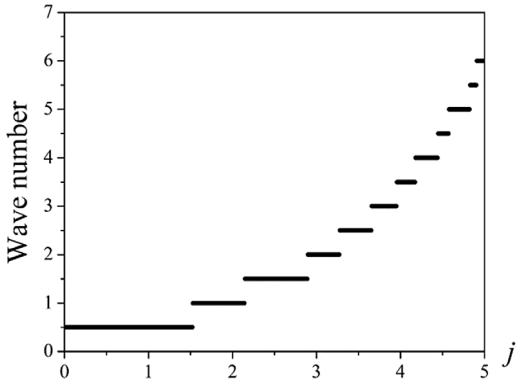

Fig. 4. The dependence of the wave number on the stiffness of the elastic medium $A_2 = 10^j$ with $A_1 = 2A_2$.

Table 2
The relation between wavenumber and A_2, where $A_2 = 10^j$.

j	Wavenumber
0–1.52	0.5
1.53–2.14	1
2.15–2.89	1.5
2.90–3.27	2
3.28–3.65	2.5
3.66–3.95	3
3.96–4.17	3.5
4.18–4.44	4
4.45–4.57	4.5
4.58–4.90	5
4.91–5	5.5

in Fig. 3. The critical buckling load $P = \sqrt{4A_2}$ is used as the compressive force here.

When the matrix stiffness is small ($A_2 = 10$), the buckled amplitude is large, and the shape of the rod resembles Euler buckling. As A_2 increases, wave numbers increase and the magnitudes of the displacement decrease. For example, the wave numbers of the rod with $A_2 = 10$, 100, 1000, 10 000 and 100 000 are 1, 2, 3.5, 4 and 6, respectively. To further understand the relation between wave number and the relative stiffness of the elastic media and the rod, the wave number is plotted against the media stiffness A_2 with $A_1/A_2 = 2$ in Fig. 4. Other parameters are the same as those in Fig. 3. The wave number of the rod increases monotonically with A_2. The transition value of A_2 is given in Table 2.

3.3. Effect of interface position

Fig. 5 shows the influence of the interface position on the rod, and the buckled shape is plotted for different interface positions $L_1 = 0.3, 0.5, 1.0, 1.5$ and 1.7 of the two layer elastic matrix. The normalized stiffness of the elastic media in layer 1 and layer 2 are $A_1 = 1000$ and $A_2 = 2000$, respectively. The normalized length of the rod is fixed as 2. The total longitudinal displacement is fixed as 0.005. The normalized compressive force P is chosen as the critical buckling load $2\sqrt{1000} \approx 64$.

Several interesting and unusual phenomena can be observed in this plot. First, the interface position does not have much effect on the wave numbers. In this range of the interface positions, the wave number of the rod stays at 2. Second, the amplitude distribution of the rod's transverse displacement U changes with the interface position. For small L_1 ($L_1 = 0.3, 0.5$), the amplitude of U is larger in layer 1 and smaller in layer 2. As the interface position increases ($L_1 = 1.5, 1.7$), the amplitude of U increases in layer 2 and decrease in layer 1. This is reasonable because increasing the interface position is similar to reducing the stiffness of the media due to $A_1 < A_2$. To maintain the same applied force at two ends, layer 2 as the stiffer part must provide larger support.

3.4. Effect of the compressive force

When supported by an elastic medium, a rod can sustain a force larger than its original critical buckling load. Fig. 6 plots the shape of the rod under different compressive forces $P = (1.05, 1.2, 1.5)\times P_{cr}$ and shows how the rod can change its shape as the compressive force increases at the post-buckling stage. When the rod just starts to buckle ($P = 1.05P_{cr}$), the displacement in layer 1 is larger than those in layer 2 due to the smaller stiffness of layer 1. For slightly

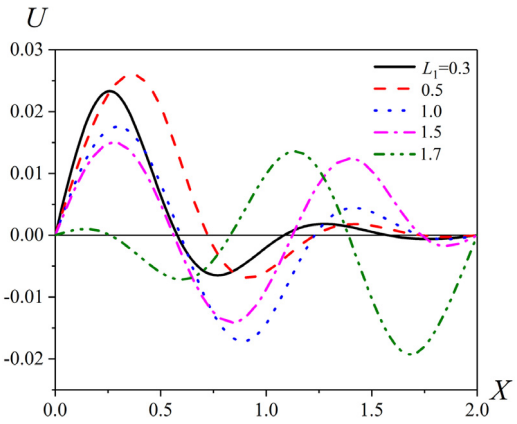

Fig. 5. The shape of the rod for different interface position embedded in a bilayer elastic medium.

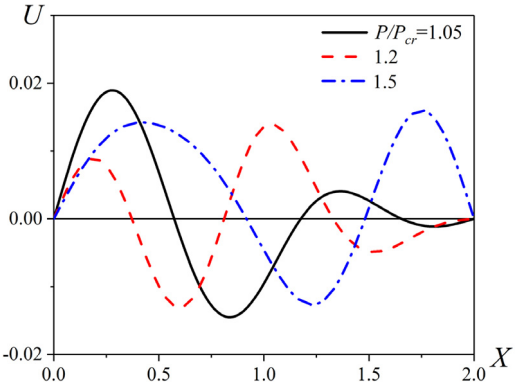

Fig. 6. The shape of a rod embedded in a bilayer elastic medium with different forces applied.

increased compressive force $P = 1.2P_{cr}$, the rod can sustain the force by slightly increasing the displacement of layer 2 and decreasing its displacement in layer 1. For large force $P = 1.5P_{cr}$, the rod must reduce its wave number from 2 to 3/2 in order to generate a larger displacement in the stiffer layer.

4. Discussion

The essential difference between the current and previous work lies in the fact that the elastic media is not uniform throughout. One important issue is the relationship between the stiffness α and the Young's modulus E of the medium. The stiffness of the elastic media was estimated as $\alpha = \frac{4\pi G}{\ln(2l/d)}$, where G the Young's modulus of the surrounding matrix, d the diameter of the rod, l the wavelength of the rod after buckling [2]. However, l cannot be determined *a priori*. By comparing the results of a 3-D elasticity approach and "Elastic rod approach", an estimation of α was obtained as: $\alpha = 2.8\pi\mu_0$, where μ_0 is the shear modulus of the surrounding matrix [15]. This result shows that the stiffness of the matrix is independent of the length and diameter of the rod. By comparing the experimental results and theoretical model used in our work, the stiffness of soft elastic medium can be estimated roughly as the α_1 and α_2 shown in Table 1.

The buckling of a beam embedded in granular media was studied and two characteristic penetration ratios a_{c1} and a_{c2} were proposed to estimate the effectiveness of the granular media as an additional clamped boundary condition [21]. In our work, the total displacement in the different layers were calculated and the 95% displacement position $L_{0.95}$ is identified for the different stiffness of the two layers.

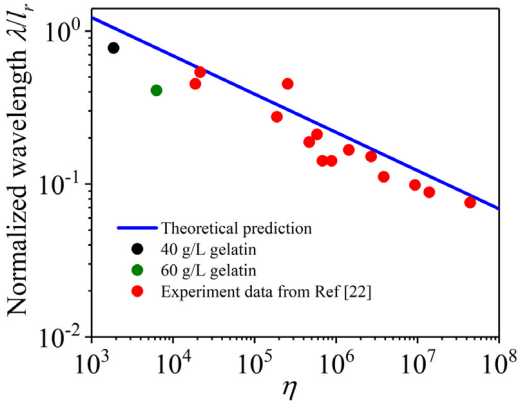

Fig. 7. Normalized buckling wavelength λ/l_r as a function of the dimensionless matrix stiffness η.

The bending rigidity and the matrix stiffness define a critical length scale of the buckling waves. For a slender rod embedded in homogeneous elastic medium, Su et al. (2014) [22] found that the wavelength λ can be estimated as $\lambda/l_r = 6.88\eta^{-1/4}$, where l_r is the length of the rod and $\eta = E_m l_r^4/E_r l_r$ is the dimensionless matrix stiffness. Jiang and Zhang (2018) [3] obtained an almost identical prediction for the wavelength: $\lambda/l_r = 6.62\eta^{-1/4}$ using an energy approach. As can be observed in Fig. 1(e) and (f), the normalized wavelengths of the rod in 40 g/L and 60 g/L gelatin are 0.77 and 0.41, respectively. Fig. 7 shows that the normalized buckling wavelength λ/l_r as a function of the normalized matrix stiffness. The solid curve shows the theoretical prediction $\lambda/l_r = 6.88\eta^{-1/4}$. The dark and green circles show the experimental wavelength of rod in 40 g/L and 60 g/L single layer gelatin respectively. Red circles show the experimental data from [22]. The dimensionless matrix stiffness we used are smaller than those used in [22]. It can be seen that our experimental wavelengths agree well with the theoretical predictions. However, there are some discrepancies, which may due to the boundary effect. As η is small, the normalized wavelength decreases to around 1, which means that there is almost only one complete buckling wave. Thus the boundaries will play a more important role and affect the wavelength. The normalized wavelengths of rod in 40 g/L (top)-60 g/L (bottom) and 60 g/L (top)-40 g/L (bottom) bilayered hydrogel are 0.45 and 0.32, respectively, which are around half of the wavelength when the rod is embedded in 40 g/L hydrogel. This may be because the stiffer layer acts as a clamped boundary condition and the effective rod length is about half of the original rod length.

In experiments, the gelatin was formed with a rod embedded in the fabrication process. Thus, the embedded element algorithm was used in Abaqus simulation, which has a reasonable representation of our experimental setup and can be used in geometrically linear or nonlinear analysis. However, in order to get an analytical solution via theoretical modeling, the longitudinal coupling between rod and the matrix is neglected and the elastic matrix is treated as an arrays of spring with stiffness α acting solely in radial direction, similar to the work in [2,22]. Besides the two above boundary conditions between rod and matrix, i.e., no sliding and free sliding, the rod may also be able to slide inside the matrix with non-negligible friction force. For example, if the gel is not fully crosslinked due to short gelling time, the bonding between the rod and the matrix is not good enough and the rod is able to slide inside the matrix with non-negligible frictional force. In another situation, when the prescribed end displacement increases, the buckling

amplitude increases correspondingly, until the rod/medium interface fractures as studied by [23]. The coupling between the rod and matrix in unfractured and fractured zone will be different, but it is outside the scope of this study.

Last but not least, it is worth pointing out the limitations of the current study and the implications for future research. Although this work considers multilayer nature of elastic medium, it does not consider anisotropy, time-independent viscoelasticity and nonlinearity. Many supporting mediums are composites and exhibit nonlinear behaviors. For instance, the cytoplasm that supports the microtubules in living cells are composites and inherently nonlinear [24], and the soil that plant roots grow in is anisotropic [6]. It has been shown that soft matrices exhibit many interesting nonlinear phenomena [25–27]. The leading nonlinear term of the supporting cytoskeleton was considered and the buckling and force decay of the microtubules in cells were studied [13], and a penetration depth was also found that depends on the nonlinearity of the elastic medium. Furthermore, the force propagation and the wavelength decay are also studied without considering the nonlinearity [14]. Another assumption in our work is that the depths of both layers are sufficiently large and the longitudinal couple effect is negligible, either of which may not hold in some scenarios. For instance, the buckling behaviors of a fiber within an elastic network with a finite length was studied and it was found that shorter fibers are more difficult to buckle than longer fibers [28]. Therefore, our work opens ample revenues for future research that will further address the effects of the nonlinearity of the elastic medium, force attenuation along the rod, the influence of finite length of the rod on buckling, etc., which will bring forth new insights into this set of highly nonlinear mechanics problems with broad implications in engineering applications.

5. Conclusion

In summary, the buckling of a rod embedded in bilayer elastic medium is investigated using combined experimental, analytical and numerical methods. The results show that: (i) layer inhomogeneity can significantly influence the direction and magnitude of the transverse displacement; (ii) layer stiffness controls the wave length and wave number of the buckling rod; (iii) loading can significantly affect the shape of the buckling rod; with smaller waves superimposed on larger waves under large compressive force, and (iv) an additional clamped boundary condition is present due to the layer elasticity inhomogeneity which limits most of the displacement to the softer layer. This work not only helps to understand various rod buckling phenomenon in multilayered matrices, but also can find applications such as the insertion of robotic needles in soft tissue [29] and the generation of underground structures via trenchless technology [30].

Acknowledgments

Zi Chen acknowledges the support from the Dartmouth startup fund, United States, and the Branco Weiss-Society in Science Fellowship, administered by ETH Zurich, Switzerland.

Appendix A. Supplementary data

Supplementary material related to this article can be found online at https://doi.org/10.1016/j.eml.2018.10.004.

References

[1] D.A. Fletcher, R.D. Mullins, Cell mechanics and the cytoskeleton, Nature 463 (7280) (2010) 485–492.
[2] C.P. Brangwynne, F.C. MacKintosh, S. Kumar, N.A. Geisse, J. Talbot, L. Mahadevan, et al., Microtubules can bear enhanced compressive loads in living cells because of lateral reinforcement, J. cell Biol. 173 (5) (2006) 733–741.
[3] H. Jiang, J. Zhang, Mechanics of microtubule buckling supported by cytoplasm, J. Appl. Mech. 75 (6) (2008) 061019.
[4] T. Li, A mechanics model of microtubule buckling in living cells, J. Biomech. 41 (8) (2008) 1722–1729.
[5] C. Wang, C. Ru, A. Mioduchowski, Orthotropic elastic shell model for buckling of microtubules, Phys. Rev. E 74 (5) (2006) 052901.
[6] J.L. Silverberg, R.D. Noar, M.S. Packer, M.J. Harrison, C.L. Henley, I. Cohen, et al., 3D imaging and mechanical modeling of helical buckling in Medicago truncatula plant roots, Proc. Natl. Acad. Sci. 109 (42) (2012) 16794–16799.
[7] M.L. Kringelbach, N. Jenkinson, S.L. Owen, T.Z. Aziz, Translational principles of deep brain stimulation, Nat. Rev. Neurosci. 8 (8) (2007) 623–635.
[8] S.T. Santillan, L.N. Virgin, R.H. Plaut, Static and dynamic behavior of highly deformed risers and pipelines, J. Offshore Mech. Arctic Eng. 132 (2) (2010) 021401.
[9] L. Wang, R. Shi, F. Yuan, Z. Guo, L. Yu, Global buckling of pipelines in the vertical plane with a soft seabed, Appl. Ocean Res. 33 (2) (2011) 130–136.
[10] M. Dogterom, B. Yurke, Measurement of the force-velocity relation for growing microtubules, Science 278 (5339) (1997) 856–860.
[11] N. Wang, K. Naruse, D. Stamenović, J.J. Fredberg, S.M. Mijailovich, I.M. Tolić-Nørrelykke, et al., Mechanical behavior in living cells consistent with the tensegrity model, Proc. Natl. Acad. Sci. 98 (14) (2001) 7765–7770.
[12] G. Brodland, R. Gordon, Intermediate filaments may prevent buckling of compressively loaded microtubules, J. Biomech. Eng. 112 (3) (1990) 319–321.
[13] M. Das, A.J. Levine, F. MacKintosh, Buckling and force propagation along intracellular microtubules, Europhys. Lett. 84 (1) (2008) 18003.
[14] W. Shan, Z. Chen, C. Broedersz, A. Gumaste, W. Soboyejo, C. Brangwynne, Attenuated short wavelength buckling and force propagation in a biopolymer-reinforced rod, Soft Matter 9 (1) (2013) 194–199.
[15] S.G. O'Keeffe, D.E. Moulton, S.L. Waters, A. Goriely, Growth-induced axial buckling of a slender elastic filament embedded in an isotropic elastic matrix, Int. J. Non-Linear Mech. 56 (2013) 94–104.
[16] J. Xiao, X. Chen, Buckling morphology of an elastic beam between two parallel lateral constraints: implication for a snake crawling between walls, J. R. Soc. Interface 10 (85) (2013) 20130399.
[17] B. Alberts, A. Johnson, J. Lewis, M. Raff, K. Roberts, P. Walter, Molecular Biology of the Cell, Garland Science, New York, 2002, Classic textbook now in its 5th Edition, 2010.
[18] D.A. Angers, J. Caron, Plant-induced changes in soil structure: processes and feedbacks, in: Plant-Induced Soil Changes: Processes and Feedbacks, Springer, 1998, pp. 55–72.
[19] J. Zhou, Y. Fung, The degree of nonlinearity and anisotropy of blood vessel elasticity, Proc. Natl. Acad. Sci. 94 (26) (1997) 14255–14260.
[20] Y. Bai, Q. Bai, Subsea Pipelines and Risers, Elsevier, 2005.
[21] A.R. Mojdehi, B. Tavakol, W. Royston, D.A. Dillard, D.P. Holmes, Buckling of elastic beams embedded in granular media, Extreme Mech. Lett. 9 (2016) 237–244.
[22] T. Su, J. Liu, D. Terwagne, P.M. Reis, K. Bertoldi, Buckling of an elastic rod embedded on an elastomeric matrix: planar vs. non-planar configurations, Soft Matter 10 (33) (2014) 6294–6302.
[23] A.M. Nasab, D. Wang, Z. Chen, W. Shan, Buckling shape transition of an embedded thin elastic rod after failure of surrounding elastic medium, Extreme Mech. Lett. 15 (2017) 51–56.
[24] M.Z. Jin, C.Q. Ru, Localized buckling of a microtubule surrounded by randomly distributed cross linkers, Phys. Rev. E 88 (1) (2013) 012701.
[25] C. Storm, J.J. Pastore, F.C. MacKintosh, T.C. Lubensky, P.A. Janmey, Nonlinear elasticity in biological gels, Nature 435 (7039) (2005) 191–194.
[26] D. Wang, M. Wu, Poynting and axial force–twist effects in nonlinear elastic mono-and bi-layered cylinders: Torsion, axial and combined loadings, Int. J. Solids Struct. 51 (5) (2014) 1003–1019.
[27] D. Wang, M. Wu, Generalized shear of a soft rectangular block, J. Mech. Phys. Solids 70 (2014) 297–313.
[28] Y. Zhao, J. Li, Y.P. Cao, X.Q. Feng, Buckling of an elastic fiber with finite length in a soft matrix, Soft Matter (2016).
[29] R.J. Webster, J. Memisevic, A.M. Okamura, Design considerations for robotic needle steering, in: Proceedings of the 2005 IEEE International Conference on Robotics and Automation, 2005. ICRA 2005, IEEE, 2005, pp. 3588–3594.
[30] S.R. Kramer, W.J. McDonald, J.C. Thomson, An Introduction to Trenchless Technology, Chapman and Hall, London, 1992.